

Condition of Optical systems Independent of Frequency for Wide Field-of-View Radio Telescope

Hiroaki Imada, Makoto Nagai, Masumichi Seta, Masaru Kino, Shun Ishii and Naomasa Nakai

Abstract—We present a condition of optical systems independent of frequency. We have known the condition independent of frequency in case of a single Gaussian beam on an optical axis, but have not known one in case of a beam propagated off the axis or tilted beam, which appears in a wide field-of-view telescope. We first show relations between an arbitrary electric field on an object and induced one after passing through a lens with calculating Fresnel diffraction. If the lens formula is met, there is a one-to-one correspondence between points on the object and image plane. This result shows we can use methods of the geometrical optics. The condition and relations derived here are confirmed by simulation. We also apply them to a wide field-of-view telescope.

Index Terms—Physical theory of diffraction

I. INTRODUCTION

WIDE field-of-view (FOV) telescopes for observing in sub-mm or THz region have been and are being developed, e.g. SPT [1], ACT [2] and CCAT [3]. In optical and infrared region, telescopes with FOV of more than 1 degree were developed e.g. Schmidt telescopes or designed using geometrical optics, e.g. [4].

There are a few characteristics of a wide field of view. First, in general, wide FOV systems have many mirrors to cancel the aberrations, not only to transmit beams. Second, we can now use a free-form surface e.g. [5], which allows us to have more choice in designing optical systems. Finally, beams propagate various paths, i.e. most of them are kept away from and tilted against the optical axis. It means that a concept of “pupil” grows greatly important.

We now focus on influence of diffraction seen in a wide FOV system. It has not been studied sufficiently in both radio and optical regions. In case of the Gaussian beam, according to [6], the beam radius at specific positions does not depend on frequency in case that the Gaussian beam propagates on the optical axis. The conditions showed in [6] are not sufficient when we apply them to a wide FOV system due to the characteristics above. We have to find applicable conditions of

a wide FOV system.

Reference [7] calculated an electric field induced by an arbitrary electric field expanded into a summation of fundamental and higher order mode Gaussian-Hermite beams. Using beam-mode transfer matrices of quadratic surface mirrors (lens), [7] showed that the distribution on the image plane can be calculated by scaling or magnifying that on the object plane without depending on frequency in case that the two planes met the lens formula. Relation of wavefront between the object and image plane, however, cannot be acquired unless the electric field is expanded into a summation of Gaussian-Hermite beams.

We can use the Fresnel diffraction integral instead of expansion of the electric field and using beam-mode transfer matrices. Reference [8] showed the calculation of the Fresnel integral but did not integrate on the object plane or take into consideration finally quadratic terms present in the phase terms.

We would like conditions, relations or equations applicable to a wide FOV system as simply as possible. It is shown that an electric field on the image plane is calculated by Fresnel diffraction integral on a single lens and the object plane and that the relation is investigated between the object and image plane in Section II. Relations between the Geometrical optics and the derivation in Section II are treated briefly in Section III. Numerical simulations verify the condition and equation derived here in Section IV and shows in Section V that we can apply them to a wide FOV telescope.

II. CALCULATING FRESNEL DIFFRACTION INTEGRAL

Fig. 1 represents the model for calculating the Fresnel diffraction integral. The xyz -coordinate is set as shown in Fig. 1 and an electromagnetic wave with a wavenumber of k propagates from the negative region of z to the positive. There is an axially symmetric lens at $z = 0$ with a radius of R , a focal length of $f > 0$ and no aberrations. We refer to the plane at $z = a$ as an object plane and to the plane at $z = b$ as an image plane, respectively. We now consider only in case of $a < 0$ and $b > 0$. (ξ_1, η_1) and (ξ_2, η_2) represent the coordinate on the object and image plane, respectively. $E_{\text{obj}}(\xi_1, \eta_1)$, $E_{\text{ins}}(x, y)$ and $E_{\text{img}}(\xi_2, \eta_2)$ are the field expressed by a complex number on the object plane, lens and image plane, respectively. The time dependence is assumed as $\exp(-i\omega t)$, where $i = \sqrt{-1}$.

Manuscript received 1 June 2014

H. Imada, M. Nagai, M. Seta and N. Nakai are with University of Tsukuba, Tsukuba, Ibaraki 305-8571 Japan (corresponding author to provide phone: +81-29-853-5600 (ext.8299); e-mail: s1330093@u.tsukuba.ac.jp).

M. Kino is with Kyoto University, Kyoto, Kyoto 606-8502 Japan.

S. Ishii was with University of Tsukuba. He is now with the University of Tokyo, Mitaka, Tokyo 181-0015 Japan

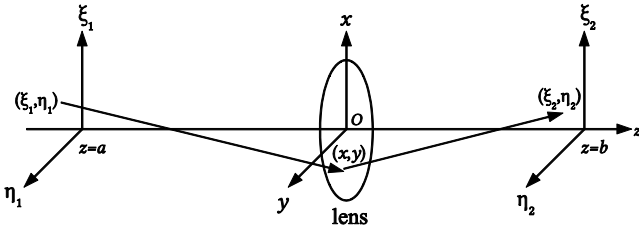


Fig. 1. Model for calculating the Fresnel diffraction integral. There is a lens with a focal length of f at $z = 0$. The plane at $z = a$ and $z = b$ is called “object plane” and “image plane”, respectively. The coordinates (x, y) , (ξ_1, η_1) and (ξ_2, η_2) are defined as shown.

Assuming the paraxial approximation which means $1/k \ll x, y, \xi, \eta, R \ll a, b, f$, paying attention to the phase transformation at the lens and using the Fresnel diffraction integral, we express the fields as follows.

$$E_{\text{img}}(\xi_2, \eta_2) = \frac{k^2}{4\pi^2 ab} \exp\left(ik(b-a) + ik\frac{\xi_2^2 + \eta_2^2}{2b}\right) \times \int d\xi_1 \int d\eta_1 E_{\text{obj}}(\xi_1, \eta_1) \exp\left(-ik\frac{\xi_1^2 + \eta_1^2}{2a}\right) \times \int dx \int dy \exp\left[-ik\frac{x^2 + y^2}{2}\left(\frac{1}{f} + \frac{1}{a} - \frac{1}{b}\right) + ikx\left(\frac{\xi_1}{a} - \frac{\xi_2}{b}\right) + iky\left(\frac{\eta_1}{a} - \frac{\eta_2}{b}\right)\right] \quad (1)$$

Equation (1) shows that the field distribution $E_{\text{obj}}(\xi_1, \eta_1)$ on the object plane and the wavenumber k define the distribution $E_{\text{img}}(\xi_2, \eta_2)$ on the image plane. We seek conditions which make the distribution $E_{\text{img}}(\xi_2, \eta_2)$ independent of the wavenumber k , that is,

$$E_{\text{img}}(\xi_2, \eta_2) = C(a, b)E_{\text{obj}}(\alpha\xi_2, \alpha\eta_2)\exp(ik\Delta), \quad (2)$$

where $C(a, b)$ and Δ are real coefficients. Evaluating the integral, we acquire

$$\frac{1}{f} + \frac{1}{a} - \frac{1}{b} = 0, \quad (3)$$

otherwise we cannot obtain the relation like (2). Equation (3) represents the lens formula. Thus, the relation is acquired,

$$E_{\text{img}}(\xi_2, \eta_2) = \frac{a}{b} E_{\text{obj}}\left(\frac{a\xi_2}{b}, \frac{a\eta_2}{b}\right) \exp\left(ik(b-a) + ik\frac{a\xi_2^2 + \eta_2^2}{2f}\right). \quad (4)$$

In case of any sign of a, b and f , (4) holds when the position a and b meet the lens formula.

III. RELATION TO GEOMETRICAL OPTICS

When we have a closer look at (4), there is a one-to-one correspondence between the points $(\xi_1, \eta_1) = (a\xi_2/b, a\eta_2/b)$ and (ξ_2, η_2) . It means that we can treat the field distribution with the geometrical optics on the plane, where the lens formula holds. Equation (4) saves us a lot of time to apply the equations introduced in [6] and [7] to a wide FOV system with many mirrors because geometrical optics allows us to know the equivalent single lens system of it which is obtained by a ray tracing simulation or by the formula combining two focal lengths of f_1, f_2 ,

$$\frac{1}{f_{\text{comb}}} = \frac{1}{f_1} + \frac{1}{f_2} - \frac{d}{f_1 f_2}, \quad (5)$$

where f_{comb} is the equivalent focal length and d is the distance between the two lens. In addition, we can apply to a complicated system with free-form surfaces whenever the ray tracing simulation tells us where the object and image plane is.

The “pupil” is one of the most important concepts in the geometrical optics. In general, various beams each propagate on their own paths in a wide FOV system except for the pupil, where all of them are piled up on the same position. The lens formula always holds on all of the pupils because they are images of one another. In addition, it is most important that the entrance pupil (Fig. 6) defines beam patterns of a telescope. When we set an electric field distribution on a specific pupil unrelated to propagating directions and apply (4) to it and the entrance (exit) pupil, the electric field distributions of all the beams are the same one and always independent of frequencies on them. Thus, a frequency-independent system is simply obtained. All we have to do is investigate where the entrance and exit pupil are with a ray tracing simulation or (5), and to determine beam parameters on the pupil.

IV. VERIFICATION OF THE RELATION

In this section, we verify the relation of (4). We apply to one spherical mirror system with a focal length $f = -150$ mm. We run an electromagnetic simulation by Grasp8 and compare simulation results with the expected one by (4). Fig 2 shows the one mirror system. Three Gaussian beams enter the mirror, on- and off-axis with a frequency of 500 GHz and off-axis with a frequency of 1 THz. The beam waists of the 500 GHz beams are located at $z = 450$ mm in Fig 2. We first investigate the field distribution of the incident beams on the plane named obj1, obj2 and obj3 at $z = 200, 300$ and 600 mm, respectively. The beams reflect and then we calculate the distribution of the reflected beams on the plane named img1, img2 and img3 at $z = 600, 300$ and 200 mm, respectively, by Grasp8 and substituting the distribution on the obj1, obj2 and obj3 for (4). Finally we compare the distribution by Grasp8 and (4).

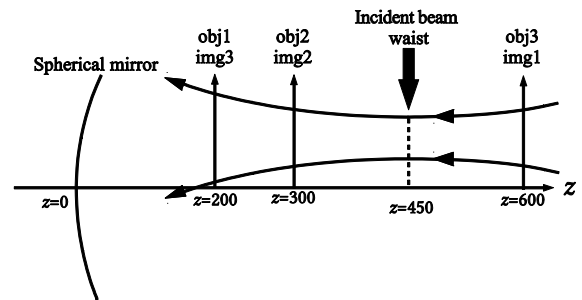


Fig. 2. One mirror simulation model. A beam propagates from the positive z axis and reflects to the same positive region.

Fig. 3 and Fig. 4 show the results for the 500 GHz beams. The electric distributions expected by (4) agree with that calculated by Grasp8 very well. The finite size of the spherical mirror affects the distribution distant from the center. The

results of calculating the phase by (4) also agree with that by Grasp8 near the center.

We also confirm whether or not the electric distributions and phase on specific position are independent of the beam frequencies. The 500 GHz off-axis beam and 1THz off-axis

beam have the same distribution and phase at the obj2. The results are shown in Fig. 5. Except for the region where the effect of the finite mirror size exists, the distribution and phase of both frequencies at the img2 shows the same shape.

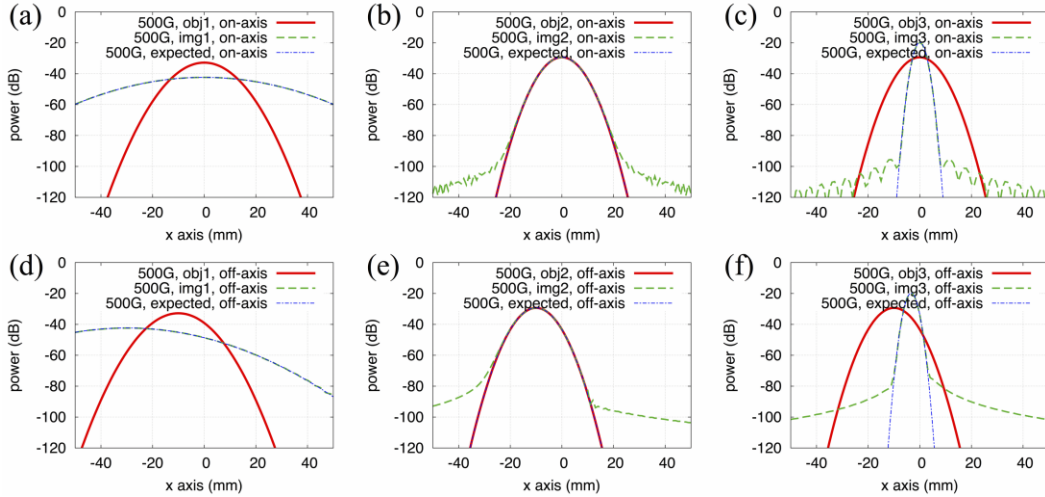


Fig. 3. Calculated electric fields on the obj and img shown in Fig. 2. The red (solid) line is the incident beam, the green (dashed) line the reflected beam by Grasp8. The blue (dashed-dotted) line is the expected distribution by (4) based on the incident beam distribution (the red-solid line). (a) 500 GHz on-axis beam investigated on the obj1 and img1. (b) 500 GHz on-axis beam investigated on the obj2 and img2. (c) 500 GHz on-axis beam investigated on the obj3 and img3. (d) 500 GHz off-axis beam investigated on the obj1 and img1. (e) 500 GHz off-axis beam investigated on the obj2 and img2. (f) 500 GHz off-axis beam investigated on the obj3 and img3.

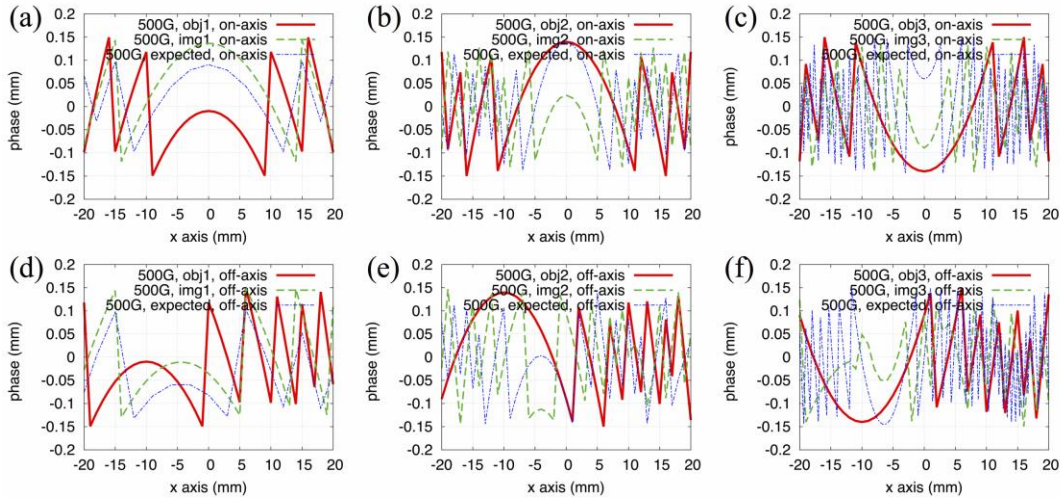


Fig. 4. Calculated phase of the electric fields on the obj and img shown in Fig. 2. The red (solid) line is the incident beam, the green (dashed) line the reflected beam by Grasp8. The blue (dashed-dotted) line is the expected distribution by (4) based on the incident beam distribution (the red-solid line). (a) 500 GHz on-axis beam investigated on the obj1 and img1. (b) 500 GHz on-axis beam investigated on the obj2 and img2. (c) 500 GHz on-axis beam investigated on the obj3 and img3. (d) 500 GHz off-axis beam investigated on the obj1 and img1. (e) 500 GHz off-axis beam investigated on the obj2 and img2. (f) 500 GHz off-axis beam investigated on the obj3 and img3.

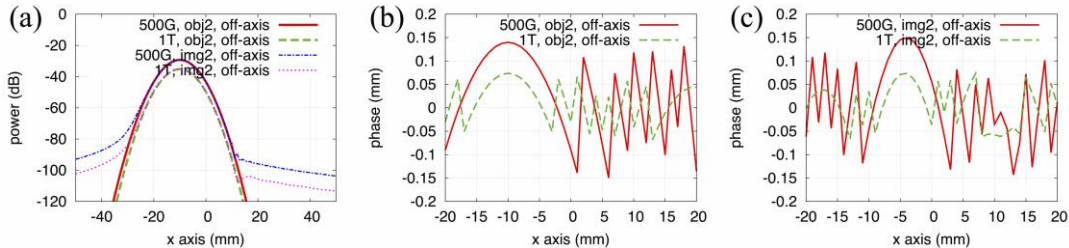


Fig. 5. The distribution and phase on the obj2 and img2. (a) The red (solid) line and green (dashed) line represent the distribution of the 500 GHz and 1THz off-axis incident beam, respectively. They are similar one. The blue (dashed-dotted) line and magenta (dotted) line is 500 GHz and 1THz off-axis reflected beam distribution, respectively. (b) The red (solid) line and green (dashed) line represent the phase of the 500 GHz and 1THz off-axis incident beam, respectively. (c) The red (solid) line and green (dashed) line represent the phase of the 500 GHz and 1THz off-axis reflected beam, respectively. They have the same shape.

V. APPLYING TO THREE MIRROR TELESCOPE

We apply (4) to the three mirror telescope as shown in Fig. 6. The primary mirror is an off-axis paraboloid with a diameter of 300 mm. The secondary mirror is an off-axis ellipsoid. The tertiary mirror is an off-axis hyperboloid. The telescope has a focal length of about -1663 mm. This telescope has a wide FOV of 1 degree at 1 THz without vignetting. There are three pupils in this system. One of them is located at the secondary. The others are images of the secondary, the entrance and exit pupil in Fig. 6. The lens formula holds on the entrance and exit pupil because they are the images of the secondary.

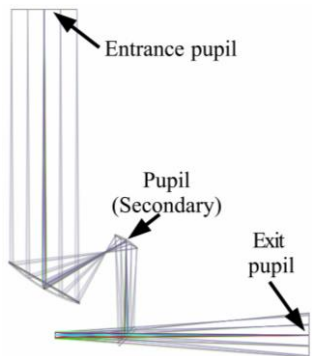


Fig. 6. Three pupils. One of them is located at the secondary.

We carry out calculations with Grasp8. Four beams pass through the telescope from the focal plane. One of them is a 500 GHz on-axis beam, the second is a 500 GHz off-axis apart from the center of the FOV, the others are the same beams as the 500 GHz ones, except for the frequency of 1 THz. An edge taper is set to be 15 dB at the secondary. According to (4), a beam radius is estimated in order to meet 15 dB at the edge of the exit pupil. A radius of curvature of wavefront is estimated from a distance between the focal plane and the exit pupil.

Fig. 7 shows the distributions on the exit and entrance pupil of the telescope. The 500 GHz and 1 THz distributions are similar on the exit pupil and keep their own shape on the entrance pupil. The fine dotted lines in Fig. 7 represent the expected distribution by (4). In this case, an equivalent a and b are -4248 mm and -1664 mm, respectively. It is shown that the field distributions on the entrance pupil do not depend on the beam frequencies. We also confirm beam patterns of this telescope. Fig. 8 shows beam patterns of the four beams in Fig. 7 on the celestial sphere. They are axially symmetric beams and have beam sizes expected from the diameter of the entrance pupil.

References

- [1] J. E. Carlstrom, P. A. R. Ade, K. A. Aird, B. A. Benson, L. E. Bleem, S. Buseti, et al., "The 10 meter south pole telescope," *Publications of the Astronomical Society of the Pacific*, vol. 123, no. 903, pp. 568–581, May 2011.
- [2] J. W. Fowler, M. D. Niemack, S. R. Dicker, A. M. Aboobaker, P. A. R. Ade, E. S. Battistelli, et al., "Optical design of the Atacama Cosmology Telescope and the Millimeter Bolometric Array Camera," *Applied Optics*, vol. 46, no. 17, pp. 3444–3454, Jun. 2007.
- [3] S. Padin, M. Hollister, S. Radford, J. Sayers, D. Woody, J. Zmuidzinas, et al., "CCAT Optics," *Proc. SPIE*, vol. 7733, 77334Y, 2010.

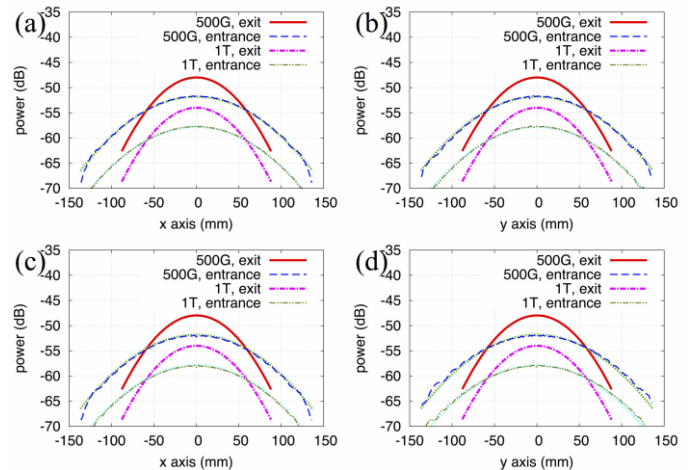


Fig. 7. Field distributions on the entrance and exit pupil. The red (solid) line is the distribution of the 500 GHz beam at the exit pupil, the blue (dashed) line is that at the entrance pupil. The magenta (dashed-dotted) and greenish brown (dashed-dotted-dotted) represents the distribution of the 1 THz beam at the entrance and exit pupil, respectively. The cyan and green (fine dotted) lines are expected from the distribution on the exit pupil. (a) The distribution along x axis of on-axis beams. (b) The distribution along y axis of on-axis beams. (c) The distribution along x axis of off-axis beams. (d) The distribution along y axis of off-axis beams.

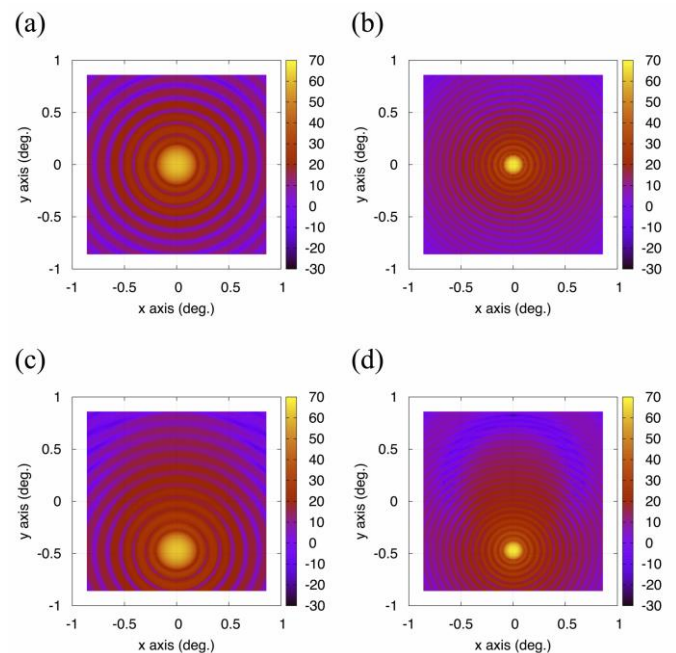


Fig. 8. Beam patterns of the telescope. (a) The 500 GHz on-axis beam. (b) The 1 THz on-axis beam. (c) The 500 GHz off-axis beam. (d) The 1 THz off-axis beam

- [4] V. Y. Terebizh, "A Purely Reflective Large Wide-Field Telescope," *Bulletin of the Crimean Astrophysical Observatory*, vol. 104, pp. 179–186, 2008.
- [5] H. Kataza, T. Wada, I. Sakon, N. Kobayashi, Y. Sarugaku, N. Fujishiro, et al., "Mid-infrared Camera and Spectrometer on board SPICA," *Proc. SPIE*, vol. 8442 84420Q, 2012.
- [6] T. Chu, "An Imaging Beam Waveguide Feed," *IEEE Trans. Antennas Propagat.*, vol. 31, no. 4, pp. 614–619, Jul. 1983.
- [7] D. H. Martin and J. W. Bowen, "Long-Wave Optics," *IEEE Trans. Microwave Theory and Techniques*, vol. 41, no. 10, pp. 1676–1690, Oct. 1983.
- [8] J. W. Goodman, *Introduction to Fourier Optics*. New York: McGraw-Hill, 1968.